Implementation of the James Webb Space Telescope Near-Infrared Camera (NIRCam) in PhoSim [Preliminary]

Colin Burke*

May 4, 2017

Abstract

In this work I leverage the existing validation of PhoSim to model the James Webb Space Telescope Near-Infrared Camera (NIRCam). This work is expected to be released shortly with PhoSim version 3.7. Simulations of images across the entirety all four of NIRCam's focal planes, and a detailed analysis of the point-spread-functions are presented. This document is useful for those wishing to gain a detailed understanding of the NIRCam implementation in PhoSim. This work is prepared prior to the pre-launch Optical Telescope and Integrated Science testing planned for Summer 2017 and is expected to be used during the in-obit testing in 2018. Usefulness for photometric algorithm calibration and general observing is also explored.

1 Introduction

The Near-Infrared Camera (NIRCam) is one of the four science instruments located within the integrated science and instrument module (ISIM) aboard NASA's next-generation flagship observatory, the James Webb Space Telesceope (JWST). The ISIM, along with the other optical component of JWST, the optical telescope element (OTE), describes the entire JWST optical system (Gardner, 2006). NIRCam is a duel-channel optical system with two "fully redundant" and "functionally identical" modules, denoted A and B (Greene, 2012). Its science goals include the study of young galaxies, distant supernovae, gravitational lensing, protoplanetary disks, and exoplanets (STScі, 2017; Gardner, 2006). These observations and potential discoveries may have significant implications for many areas of astrophysics and cosmology that align with our group's particular interests. In this work, I simulate the OTE and NIRCam as a comprehensive, end-to-end model of the optical prescription.

This work is of interest to the devlopment of PhoSim because JWST is a diffraction-limited space telescope, unlike the Large Synoptic Survey Telescope (LSST), for which PhoSim was originally designed. In addition, JWST/NIRCam is by far the most complex

*Purdue University, Department of Physics and Astronomy, West Lafayette, IN, 47907. Please email colin.burke.j@gmail.com.

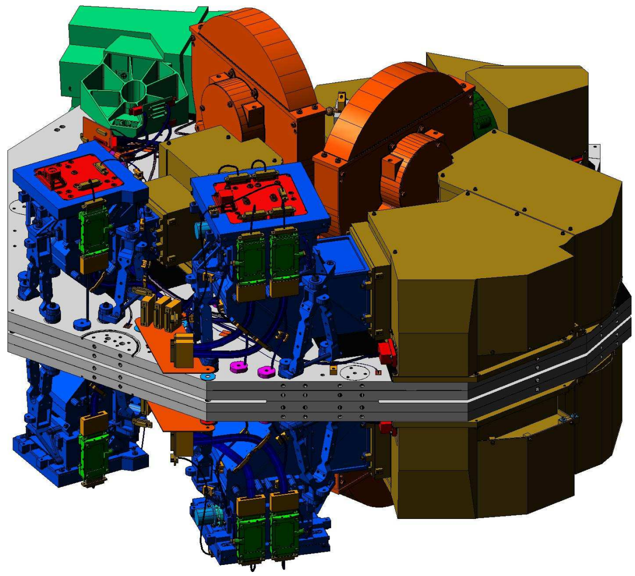

Figure 1: Rendering of NIRCam showing both modules and all four FPAs (from STSci, 2017).

optical system ever modeled with PhoSim. Thus, I demonstrate the flexilbilty of PhoSim in a vastly different case from previous PhoSim implementations.

Although other tools exist to model the optical behavior of NIRCam, none present a cohesive, end-to-end, physics-based simulation like PhoSim. NIRCam is the primary imaging instrument on-board JWST. Thus, an implementation of NIRCam in PhoSim is expected to be of significant interest to the JWST community.

2 Implementation

2.1 Optical Prescription

Table 1: PhoSim ISC directories.

directory name	description
`nircam_sw`	short wavelength (SW) channel
`nircam_lw`	long wavelength (LW) channel

The NIRCam optical design is stored and analyzed by optical engineers using Zemax software. I obtained the Lockheed Martin flight-ready optical design in the form of two Zemax lens files (`L050713FLT.zmx` and `S050713FLT.zmx`) from Jarron Leisenring at the University of Arizona Department of Astronomy and Steward Observatory. The Zemax lens files contain a complete description of the optical system where spatial coordinates of each surface are defined sequentially (Zemax, 2011). Because NIRCam is a duel-channel system, one file describes the long-wavelength (LW) channel, while the other describes the short-wavelength (SW) channel. Light is bifurcated into both channels via the dichroic beam

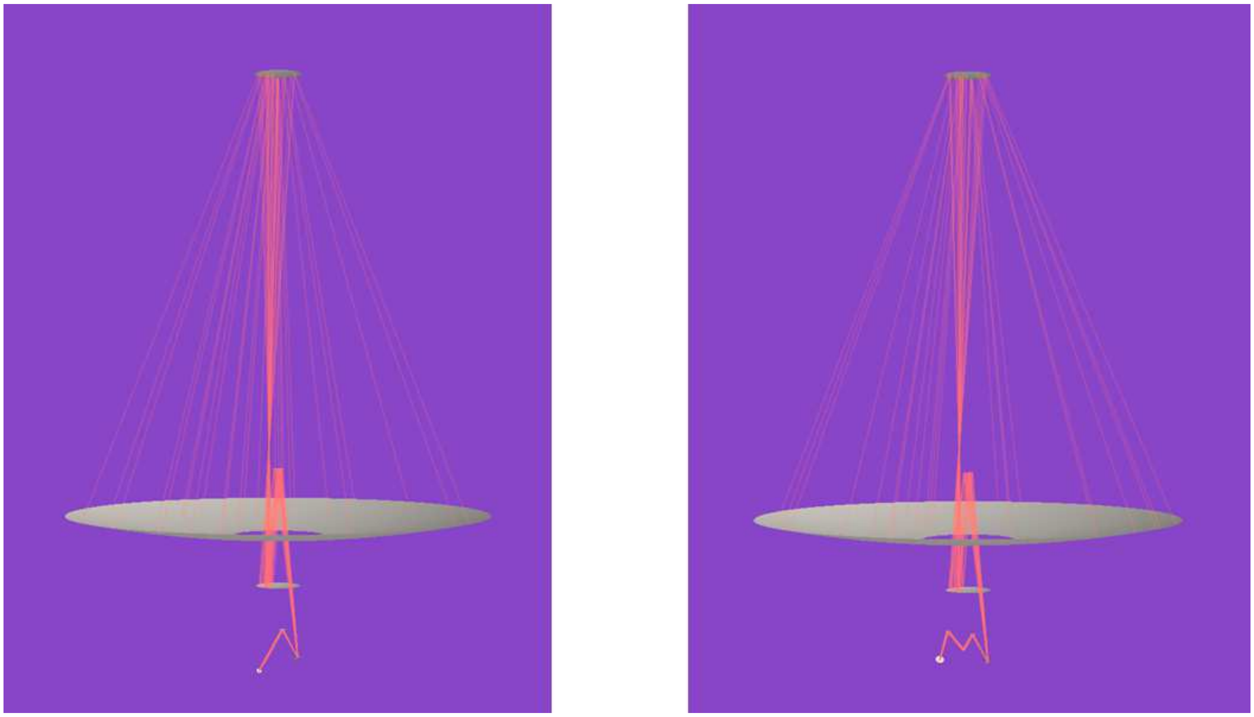

Figure 2: Visualization of a PhoSim raytrace through the OTE and NIRCam SW (right) and LW (left) channels.

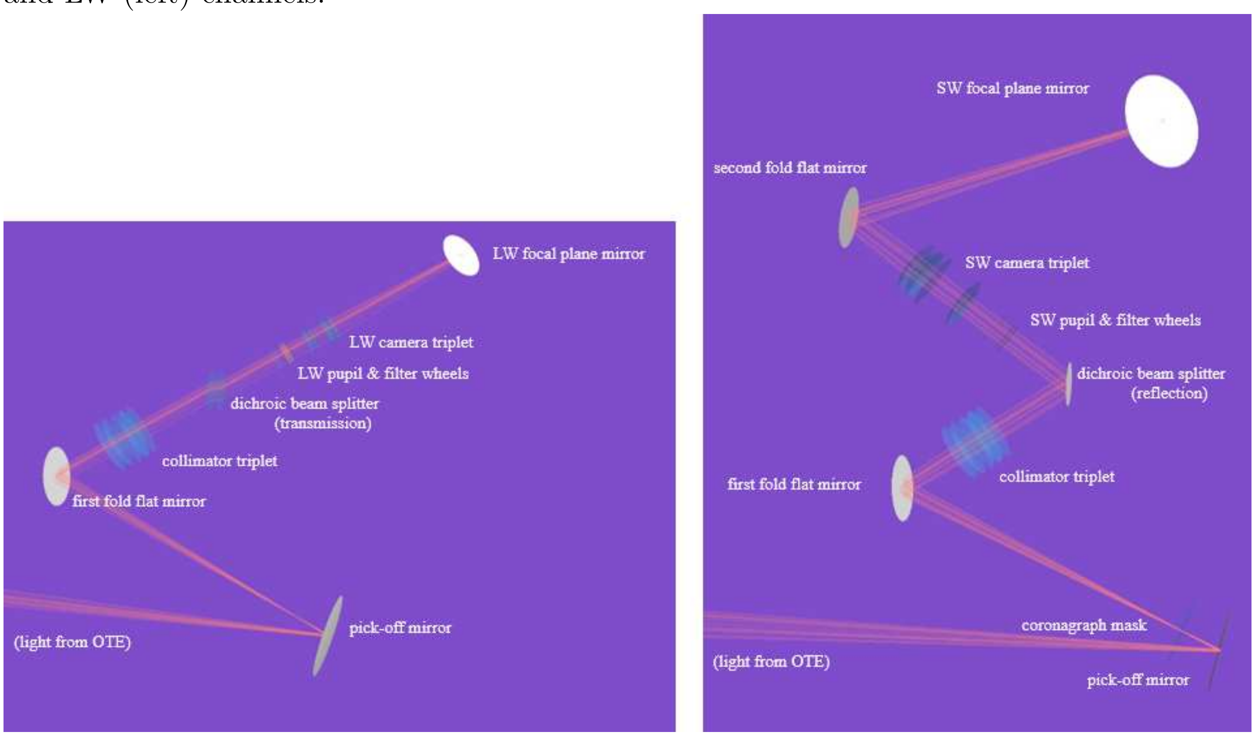

Figure 3: Close-up of a PhoSim raytrace through the NIRCam SW (right) and LW (left) channels. (Focal planes are not shown, but lie adjacent to the focal plane mirrors.)

splitter (DBS), and is projected onto two focal planes (Figures 2 and 3). The plate scales are 0.0317"/pixel and 0.0648"/pixel for the SW and LW channels respectively (STSci, 2017). Although the modules are functionally identical, there are slight differences with respect to the detectors and throughput shown in §2.2 and §2.3. Because of these differences, we also separate the PhoSim implementation for each channel in the form of two instrument and site characteristic (ISC) directories. These two directories contain various files with all the details of the optical prescription for PhoSim. Although the NIRCam modules are adjacent to each other, this is irrelevant for all raytracing and physics. But we must consider the different orientations of the images on the focal planes (Figure 4). While this approach simplifies the simulations, the drawback is PhoSim cannot easily run simulations simultaneously for both channels.

The ISC directory file structure is described in Table 2. Both models have identical file structure, although some details in the files themselves differ. An asterisk (*) indicates the file is not currently used in this version.

Table 2: PhoSim ISC directory file structure.

file/directory name	description
`throughput/`	Directory for ThroughtputFiles which specify the total system throughput for each filter mode (§2.5).
`optics_x.txt`	OpticsFile: describes the optical prescription for filter mode `x` (Tables 7 and 8).
`perturbation.txt`	PerturbationFile: optical element coordinates and future perturbation models (Tables 9 and 10).
`focalplanelayout.txt`	FocalplaneLayoutFile: describes the layout of the focal plane (Tables ?).
`chipmaterial.txt`	ChipMaterialFile: specifies the chip material and other detailed variables `x` (Tables ?).
`segmentation.txt`	SegmentationFile: details amplifier readout segmentation (Figure 4).
`tracking.txt`	TrackingFile: specifies the jitter model(s) to use and their input values*.
`actuator.txt`	ActuatorFile: for active optics*.
`pupilscreen.fits`	DiffractionScreenFile: JWST pupil data for diffraction calculation (Figure 6).
`BaF2_37K.txt`	CoatingFile for Barium Fluoride (§2.1.1).
`LiF_37K.txt`	CoatingFile for Lithium Fluoride (§2.1.1).
`ZnSe_37K.txt`	CoatingFile for Zinc Selenide (§2.1.1).
`Si_30K.txt`	CoatingFile for Silicon (§2.1.1) *Only LW channel.*.
`F_Silica.txt`	CoatingFile for fused silica (§2.1.1). *Only SW channel.*

In detail, the OTE contains the primary mirror (PM), secondary mirror (SM), tertiary mirror (TM), fine steering mirror (FSM), and the pick-off mirror (POM). In this case, the POM directs light into NIRCam. NIRcam itself contains the collimator lens triplet (colij) and the DBS (DBS or DBSij), before being split into both channels. Each channel contains a pupil wheel surface (SWPij or LWPij), filter wheel surface (SWFij or LWFij), a flat focal plane mirror (SWFPM or LWFPM), a camera lens triplet (SWij or LWij) and the focal plane itself. In addition, the SW channel contains a second flat fold mirror (SFF) in-between SW32 and SWFPM. For optical elements with two surfaces (e.g., front and back of a lens), j denotes surface $j = 1$ or $j = 2$. i distinguishes the optical element in a lens group.

The optics files were created by direct conversion from the Zemax lens files and their associated prescription data report Zemax outputs (which are much easier to read), using the scripts in the tools directory (`ZMXtoPhosim.py` and `prescriptionDataToPhosim.py`). There are various optics files in each ISC directory, each corresponding to a NIRCam filter mode (Table 8).

2.1.1 Optical Materials

Five materials are modeled in PhoSim for NIRCam, BaF_2, LiF_2, ZnSe, Si, and fused silica. The cryogenic indicies of refraction for each material are described by either the Sellmeier equation (Sellmeier, 1871):

$$n^2(\lambda) = 1 + \frac{B_1\lambda^2}{\lambda^2 - C_1} + \frac{B_2\lambda^2}{\lambda^2 - C_2} + \frac{B_3\lambda^2}{\lambda^2 - C_3} \tag{1}$$

or the Schott equation (Zemax, 2011):

$$n^2(\lambda) = a_o + a_1\lambda^2 + a_2\lambda^{-2} + a_3\lambda^{-4} + a_4\lambda^{-6} + a_5\lambda^{-8}. \tag{2}$$

The coefficients are given in the Zemax ASCII glass catalog file (extension .AGF), and are shown in Tables 3 and 4.

Table 3: Sellmeier Equation Coefficients.

material name	B_1	B_2	B_2	C_1	C_2	C_3
BaF2_37K	4.792460446e−1	1.945485193e−3	6.798570853e−1	1.069046281e−2	3.868534430e+0	2.160578579e+3
LiF2_37K	−9.252453221e−3	7.415406159e−3	9.419588365e−1	5.189131445e−3	5.197440041e+0	7.977281530e+2
ZnSe_37K	4.490689574e+0	4.059550473e−2	3.672737223e−1	1.546597938e−1	2.041649826e+0	1.582728449e+3
F_Silica	6.961663000e−1	4.679148000e−3	4.079426000e−1	1.351206300e−2	8.974794000e−1	9.793400250e+1

Table 4: Schott Equation Coefficients.

material name	a_0	a_1	a_2	a_3	a_4	a_5
Si_30K	1.145433421e+1	9.722579803e−9	9.086905708e−1	−2.828149436e−4	8.322888739e−4	−6.958764296e−4

2.2 Focal Plane Layout

Specifications of all five detectors are in the form of the field coordinates in the Zemax lens files. The included field coordinates specify the initial coordinates of light that are raytraced through the OTE and NIRCam in Zemax. The field coordinates specify the center of the chip 5 (LW), and the corners in-between chips 1, 2, 3, and 4 (SW). The position of each chip can then be obtained simply by projecting these coordinates onto the focal plane via raytrace, and fixing each chip at the raytraced coordinates on the focal plane. In this work, I also assume that the rotation of each chip is the same as the rotation of the focal plane surface for the corresponding channel.

The position and orientation of both focal planes are specified in their respective PerturbationFiles. For the SW channel, the dx and dy values for all 4 chips are specified in the FocalplaneLayout file with their positions and orientations all set to 0 in this file. This is the recommended way to place focal planes with non-trivial orientations so the trim routine works and FITS World Coordinate System (WCS) output is correct. This way, the dx and dy values are applied after the rotation in the PerturbationFile, ensuring the `CRPIX` WCS header keywords are calculated properly.

It is possible that a more detailed description of the chip coordinates on the focal plane exists, however it is always a challenge to place each chip with the proper coordinates and rotation precisely. Finally, I crudely adjust each chip defocus such that the point-spread-function (PSF) root mean square (RMS) radial size is at a rough minimum across all wavelengths and field positions.

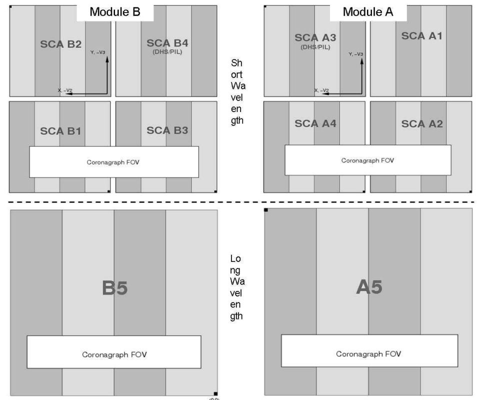

Figure 4: Layout of the chips on each focal plane. The black squares correspond to the start of the readout process and the different shaded regions represent the amplifier output channels (from STSci, 2017).

Table 5: Intrensic SW chip offsets [mm].

chip #	x	y
1	19206	19872
2	20052	-19278
3	-19782	19170
4	-19440	-19836

Each chip is approximately 8 μm thick (M. Rieke, private communication) and has a total resolution of 2048 $\times$ 2048. But each chip has an active detection area of 2040 $\times$ 2040 pixels due to the 4 reference pixels along each edge (Loose, 2007). The `focalplanelayout.txt` ISC file describes NIRCam's focal planes accordingly.

2.3 Detector Physics

NIRCam's ten 2048$\times$2048 pixel HAWAII-2RG (H2RG) complementary metal-oxide-semiconductor (CMOS) detectors are composed of Mercury Cadmium Telluride (MCT), $Hg_{1-x}Cd_xTe$, with different relative compositions of Cd x (Loose, 2007). This allows for a tunable bandgap, which corresponds to a variable cutoff wavelength λ_{co}. Considerable effort has been made to understand the optical properties and electron interactions of HgCdTe photodetectors in recent decades (Rogalski, 2005; Itsuno, 2012). We have implemented MCT detectors in PhoSim, which calculates the photon mean free path from the absorption coefficient for a given x.

PhoSim simulates all relevant physics of CMOS (and CCD) detectors in a multi-step photon-to-electron conversion code. A final image is produced with highly realistic results (Peterson et al., 2015). However, prior to PhoSim version 3.6, only silicon detectors were implemented. To model the absorption coefficient in MCT as a function of photon wavelength, I first make use of the following equation given by Hansen et al. (1982):

$$E_g(x, T) = -.302 + 1.93x + 5.53(10^{-4})T(1 - 2x) - 0.810x^2 + 0.832x^3 \tag{3}$$

where E_g is the bandgap energy in eV, T is the temperature in K, and x is the relative composition of Cd.

Applying the Planck-Einstein relation, $E_g = hc/\lambda_{co}$, Equation 3 can be re-expressed in terms of the cutoff wavelength, given in μm:

$$\frac{1.24\ \text{eV}\mu\text{m}}{\lambda_{co}} \cong -.302 + 1.93x + 5.53(10^{-4})T(1-2x) - 0.810x^2 + 0.832x^3. \tag{4}$$

I use the known cutoff wavelengths of both detectors, $\lambda_{co} = 2.5\ \mu$m and $\lambda_{co} = 5.3\ \mu$m (Garnett, 2004), for the SW and LW channels respectively and solve for the real root of Equation 4 with $T = 37$ K. The values obtained are $x = 0.4595$ and $x = 0.2995$ for the SW and LW chips respectively. Note that I could omit this step if measured values of x for both channels were to be provided from some other source, if they exist.

I then implement an empirical piece-wise model for the Kane region ($E_\gamma > E_g$) given by Chu et al. (1994) and the modified Urbach tail ($E_\gamma < E_g$), given by Finkman and Schacham (1984) and Hougen (1989) where E_γ is the incident photon energy:

$$\alpha = \begin{cases} \alpha_o \exp\left[\sigma\left(\frac{E_\gamma - E_o}{T+T_o}\right)\right] & E_\gamma < E_g \\ \beta\sqrt{E_\gamma - E_g} & E_\gamma > E_g \end{cases} \tag{5}$$

where the parameters are defined as:

$\alpha_o = \exp(53.61x - 18.88)$
$E_o = -0.3424 + 1.838x + 0.148x^2$
$T_o = 81.9$
$\sigma = 3.267 \times 10^4(1+x)$

$E_T = \left(\frac{T_o+T}{\sigma}\right)\ln(\alpha_T/\alpha_o) + E_o$
where $\alpha_T = 100 + 5000x$
$\beta = \alpha_T(E_T - E_g)^{-1/2}$
and E_g is specified by Equation 3.

The mean free path of a photon is simply given as the inverse of the absorption coefficient α. The conversion path length is calculated in PhoSim by multiplying the absorption coefficient by an exponentially distributed random number (Peterson et al., 2015). Both detectors are approximately 8 μm thick (M. Rieke). Figure 5 shows the absorption coefficients for MCT in PhoSim as a function of incident photon wavelength for both channels at 37 K.

I implement the model given by Lui et al. (1994) for the index of refraction in MCT as a function of λ, T, and x:

$$n = \sqrt{\frac{A+B}{1-(C/\lambda)^2} + D\lambda^2} \tag{6}$$

where the parameters A, B, C, and D are defined as:

$A = 13.173 - 9.852x + 2.909x^2 + 0.001(300-T)$
$B = 0.83 - 0.246x - 0.0961x^2 + 8 \times 10^{-4}(300-T)$
$C = 6.706 - 14.437x + 8.531x^2 + 7 \times 10^{-4}(300-T)$
$D = 1.953 \times 10^{-4} - 0.00128x + 1.853 \times 10^{-4}x^2.$

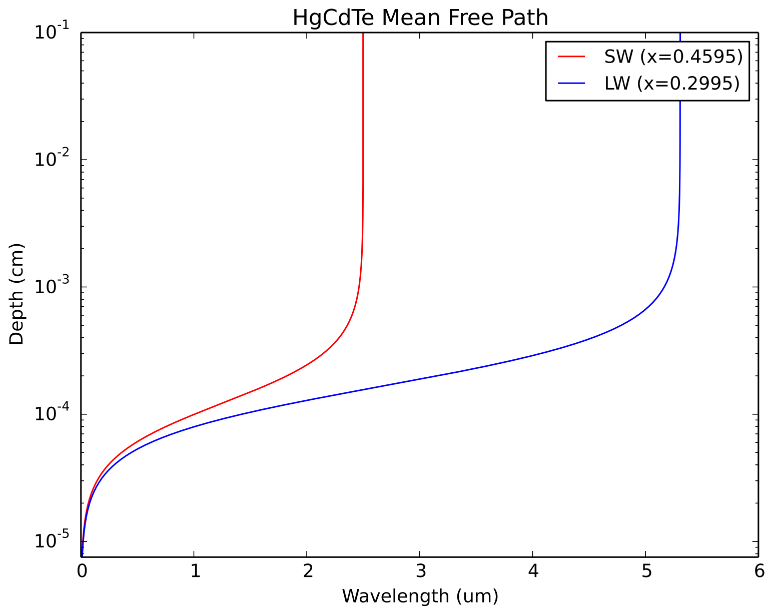

Figure 5: Plot of the mean free path for both channels as a funcition of wavelength.

In accordance with Peterson et al. (2015)[1], the electric field profile in MCT is:

$$E_z(z) = \frac{V}{t_{MCT}} + \frac{q}{\epsilon_0 \epsilon_{MCT}(x)} \int_{t_{MCT}}^{z} dz n_d(z) \tag{7}$$

where V is the overdepletion potential, t_{MCT} is the MCT thickness, $\epsilon_{MCT}(x)$ is the relative permittivity in MCT, and $n_d(z)$ is the doping density function. The relative permittivity (dielectric constant) in MCT is given in the high frequency approximation by Dornhaus et al. (1983):

$$\epsilon_{MCT}(x) = 15.2 - 15.6x + 8.2x^2. \tag{8}$$

The doping density function is given by,

$$n_d(z) = n_{bulk} + n_b e^{-\frac{(t_{MCT}-z)}{s_b}} + n_f e^{-\frac{z}{s_f}}. \tag{9}$$

The transverse diffusion is calculated with the Gaussian diffusion width, $\sqrt{2Dt_c}$, where D is the diffusion coefficient given by,

$$D = \frac{\mu_q(x,T)kT}{q} \tag{10}$$

where $\mu_q(x,T)$ is the electron mobility in MCT. For this work, I implement the model for electron mobility in MCT given by Rosbeck et al. (1982):

$$\mu_q(x,T) = \frac{9 \times 10^8 s}{100T^{2r}} \tag{11}$$

[1] I have duplicated some information from Peterson et al. (2015) here for completeness, modifying the relevant equations for the MCT material.

where $r = (0.2/x)^{0.6}$ and $s = (0.2/x)^{7.5}$. The collection time is,

$$t_c = \int_{z_c}^{z} \frac{dz}{|\mu_q(x,T)E_z(z)|}. \tag{12}$$

Further work will identify what other relevant differences may arise between silicon and MCT detectors. I also have concerns about the validity of the models presented in this section at NIRCam's cryogenic temperature of 37 K.

2.4 Diffraction

Due to the segmented "tricontagon" geometry of the JWST pupil aperture and the non-symmetric deployed configuration of the secondary mirror support structure (SMSS) spider, there are considerable challenges to specifying the layout of the PM and the SMSS in PhoSim. Because the diffraction tends to blur at multiple wavelengths and with detector noise, an easily-implemented approximation of the entrance pupil is used.

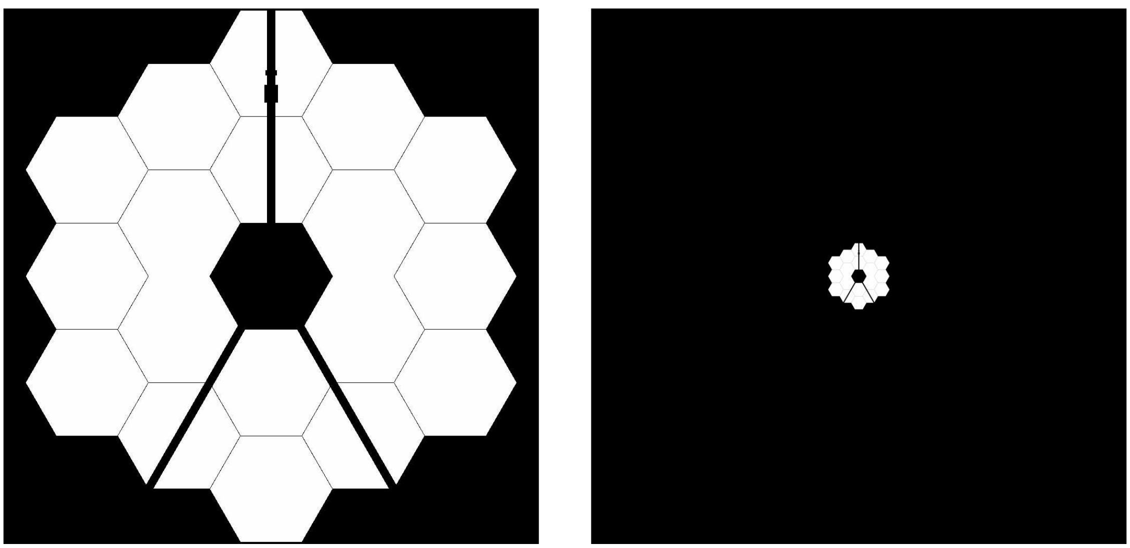

Figure 6: Image of the pupil diffraction screen used in this work, before padding (left) and after 8x padding (right). This means full-resolution pupil is scaled by $1/\gamma$ where $\gamma = 8$. Note: not shown here at full resolution.

We generate a 2-dimensional diffraction screen array from a FITS image of the revision V entrance pupil taken from the WebbPSF data files [2]. We downsample the original 1024×1024 image 8 times by scaling the pupil resolution by $1/\gamma$ where $\gamma = 8$, and pad the outside with zeros. This padding ensures the fast Fourier transform (FFT) algorithm will produce accurate results, although it decreases the effective resolution of the pupil because the screen size is limited to 1024×1024 pixels for computational effeciency. This method is similar to the diffraction calculation in WebbPSF, although it is slightly slower than their matrix formalism (Perren, 2012). However, since the typical usage for PhoSim is large-scale simulations of

[2] See <pythonhosted.org/webbpsf/>.

many sources across many chips (rather than a single PSF), PhoSim's speed is not dictated by the diffraction calculations. In addition, we are largely interested in measurements at the size of one pixel (18 μm). The approximations used in this work are further justified with the understanding that multi-wavelength analysis and other detector effects will wash out the distribution even further.

The final result is the PM shape approximated as a single circular-aperture surface for the raytracing, and is approximated with the pupil screen shown in Figure 2.4 for the diffraction. Both are convolved into the final image (Figure 7). Please see Burke (2017) for a detailed description of the modifications to the PhoSim diffraction algorithm for space telescopes such as JWST.

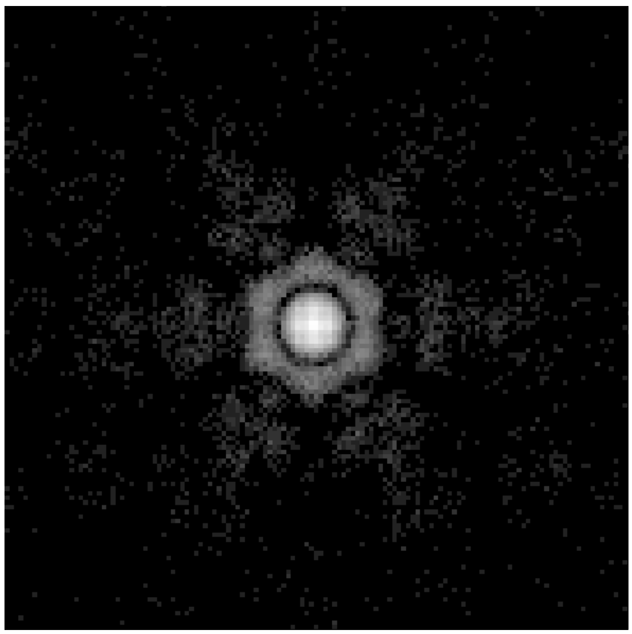

Figure 7: An example image of JWST diffraction on the detector.

2.5 Throughput

Finally, the throughput of the entire optical system minus the detector quantum efficiency is implemented from the data available from the Space Telescope Science Institute web page[3]. The user can easily select a particular filter to simulate with PhoSim (see §4.2). While every filter is implemented in this work, we have yet to add coronagraphic, wavefront sensor, spectroscopic, or calibration source modes.

More work should be done to ensure the photometry is correct (not double counting containimation throughput and placing individual throughput curves on all optcal elements).

[3]See <www.stsci.edu/jwst/instruments/nircam/instrumentdesign/filters>.

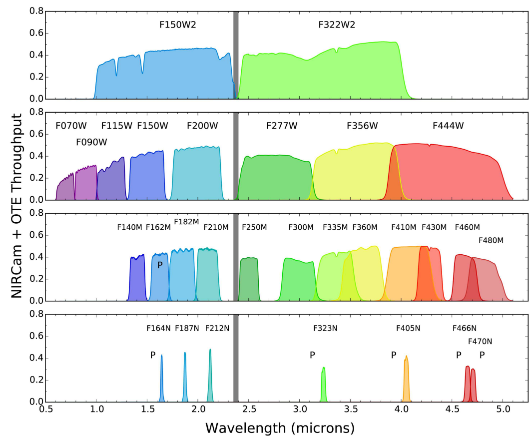

Figure 8: Plot of the throughput for each NIRCam filter (from STSci, 2017).

3 Background

The background model for JWST is comprised of zodiacal light, itself made up of two components: scattered light and thermal emission. The model is described by Rieke (2013) in the sensitivity calculations technical report. It incudes both scattered and thermal zodiacal light blackbody spectra:

$$F = \frac{3.95 \times 10^{-14} \cdot 1.19 \times 10^{8} \cdot \lambda^{-5}}{e^{14388/(\lambda \cdot 5300)} - 1} + \frac{2.79 \times 10^{-8} \cdot 1.19 \times 10^{8} \cdot \lambda^{-5}}{e^{14388/(\lambda \cdot 282)} - 1} \tag{13}$$

where λ is given in μm. The first term is the scattering and the second term is the thermal emission. The spectral energy distribution (SED) is show in Figure 11. In PhoSim, the flux is scaled depending on the telescope pointing to account for the spatial variation of zodiacal emission.

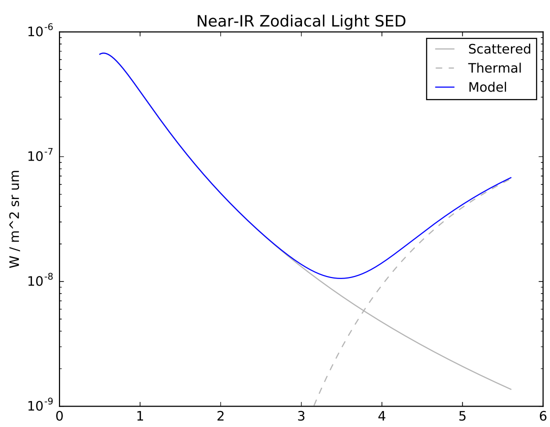

Figure 9: Plot of the zodiacal background SED used in the work.

4 Usage

4.1 Physics Commands

Due to the inherent difference in simulating space-based environments as opposed to ground-based ones, careful consideration must be made to avoid turning on unwanted physics, such as physics pertaining to the atmosphere. Thus, I invoke use of PhoSim's powerful physics override commands, which are placed inside of the CommandFiles. Four new CommandFiles are created and placed in the `examples` director to override PhoSim's default physics environment for JWST/NIRCam:

1. `noatmosphere`: The recommended command for JWST physics. This file is similar to the `nobackground` CommandFile, but it also removes the atmosphere, cools the detector to 37K, aligns the telescope to the catalog origin (see paragraph below), and simulates the diffraction with the pupil screen method described in §2.4).

2. `perfect`: Just geometric raytrace (including geometric optical distortions and multi-wavelength aberrations) with all other physics off. This is a perfect telescope with optical raytracing.

3. `dummy`: Similar to the previous CommandFile, but the geometric raytracing, along with all other physics besides diffraction, is off. This will produce geometric distortion-free images with diffraction using a dummy telescope algorithm which approximates the platescale and collapses all rays onto a point and approximating the flux given the aperture size.

4. `quickbackground`: Atmosphere is off, but all other physics plus background is turned on.

New PhoSim physics override commands (`rotatex`, `rotatey`) exist that effectively rotate the entire telescope (in degrees) to reproduce the off-axis offset of the field coordinates in Zemax. This offset exists due to the apparent off-axis OTE behavior inherent to the JWST optical design. When placed in a PhoSim CommandFile, these commands effectively move the CatalogFile coordinate origin to the Right Ascension α (RA) and Declination δ (Dec) equivalent of the `rotatex`, `rotatey` input. So the CatalogFile coordinate origin ($\alpha = 0, \delta = 0$) corresponds to this new telescope rotation. The command's values come from the .13 degree tilt included in the Zemax files and the additional offset to align the CatalogFile coordinate origin to the center of the focal planes.

A detailed understanding of these commands (and, indeed, the optical design itself) are not a requirement for the user. An understanding that the origin of the CatalogFile coordinate system corresponds to the center of the NIRCam focal planes will suffice. This is likely the expected behavior, and many users may not even be aware of the details.

4.2 Command Line Execution

To run a simulation of a single star located in the center of chip 5 with no background, one would simply run the following command:

```
./phosim examples/zmx_field5 -c examples/noatmosphere -i nircam_lw
```

To run a simulation of all focal planes using Eiichi Egami's catalog based off of an Hubble Space Telescope field with a quick background, try:

```
./phosim examples/candels_phosim_bright.cat -c examples/quickbackground -i nircam_sw
./phosim examples/candels_phosim_bright.cat -c examples/quickbackground -i nircam_lw
```

4.3 Exposure Time

The user should set the desired exposure time in the CatalogFile. There are three parameters: the visit time $t_{\text{exp.}}$, which is the total exposure time for all observations, the number of snaps N_{snaps}, which is the number of exposures in a sequence of observations, and the chip readout time t_{readout}. Thus,

$$t_{\text{exp.}} = (t_{\text{visit}} + t_{\text{readout}})/N_{\text{snaps}}. \tag{14}$$

However, for CMOS detectors the readout time is zero. So the simplest usage would be to set the number of snaps to one and then the visit time becomes the total exposure time.

4.4 Filter Selection

NIRCam contians a variety of filters and pupils in the filter and pupil wheels, shown in Figure 10. The throughput for all of NIRCams filters is implemented. The filter should be set in the CatalogFile by the user using the `Opsim_filter N`. Where `N` is the filter number corresponding to Table 6.

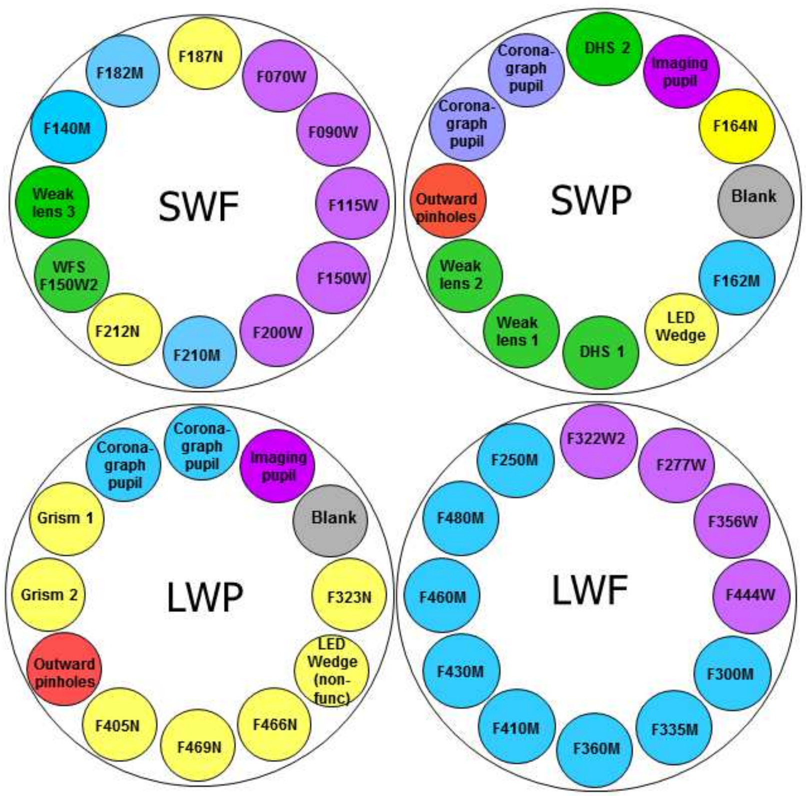

Figure 10: Visualization of the NIRCam filters and pupils (from STSci, 2017).

Table 6: PhoSim-NIRCam Filter Lookups for the SW (left) and LW (right) channels

Number	NIRCam Filter
0	No filter
1	F070W_A
2	F070W_ABmean
3	F070W_B
4	F090W_A
5	F090W_ABmean
6	F090W_B
7	F115W_A
8	F115W_ABmean
9	F115W_B
10	F140M_A
11	F140M_ABmean
12	F140M_B
13	F150W_A
14	F150W_ABmean
15	F150W_B
16	F150W2_A
17	F150W2_ABmean
18	F150W2_B
19	F162M_A
20	F162M_ABmean
21	F162M_B
22	F164N_A
23	F164N_ABmean
24	F164N_B
25	F182M_A
26	F182N_ABmean
27	F182N_B
28	F187N_A
29	F187N_ABmean
30	F187N_B
31	F200W_A
32	F200W_ABmean
33	F200W_B
34	F210M_A
35	F210M_ABmean
36	F210M_B
37	F212N_A
38	F212N_ABmean
39	F212N_B

Number	NIRCam Filter
0	No filter
1	F250M_A
2	F250M_ABmean
3	F250M_B
4	F277W_A
5	F277W_ABmean
6	F277W_B
7	F300M_A
8	F300M_ABmean
9	F300M_B
10	F322W2_A
11	F322W2_ABmean
12	F322W2_B
13	F323N_A
14	F323N_ABmean
15	F323N_B
16	F335M_A
17	F335M_ABmean
18	F335M_B
19	F356W_A
20	F356W_ABmean
21	F356W_B
22	F360M_A
23	F360M_ABmean
24	F360M_B
25	F405M_A
26	F405M_ABmean
27	F405M_B
28	F410M_A
29	F410M_ABmean
30	F410M_B
31	F430M_A
32	F430M_ABmean
33	F430M_B
34	F444W_A
35	F444W_ABmean
36	F444W_B
37	F460M_A
38	F460M_ABmean
39	F460M_B
40	F466N_A
41	F466N_ABmean
42	F466N_B
43	F470N_A
44	F470N_ABmean
45	F470N_B
46	F480M_A
47	F480M_ABmean
48	F480M_B

4.5 Intended Uses

This work is expected to be used internally by the NIRCam team at the University of Arizona prior to full-science operations. Its current intended use includes:

- Testing the data processing pipeline.
- Testing for photometry algorithms.
- Tracing of possible anomolies during in-orbit check.
- As a public tool for planning observations.

5 Analysis and Validation

5.1 Photometry

No work has been done yet to validate the photometry. More effort should be put into assuring we do not double count effects such as contamination absorption. In the future, one could plot the total flux on the detector for each filter configuration and compare this with the real telescope in an attempt to match the configurations. However, NIRCam's complicated optics and detector effects may make this more challenging than one might expect.

5.2 PSF Size

Since JWST is diffraction-limited, this provides a useful lower-bound on the PSF size. The diffraction limited RMS size is defined in terms of the focal ratio $F/\#$ as,

$$\text{RMS}_{\text{diffraction limit}} = .42(F/\#)\lambda \tag{15}$$

where the focal ratio is 18.2 and 8.9 for the SW and LW channels respectively.

Early results from detailed analysis of the PSF size indicate PhoSim is convolving the diffraction and geometric portions of the PSF in a way that results in 10-20% increase in PSF size. More work is currently underway to understand this in more detail to see if this effect is real or just a mistake in this implementation.

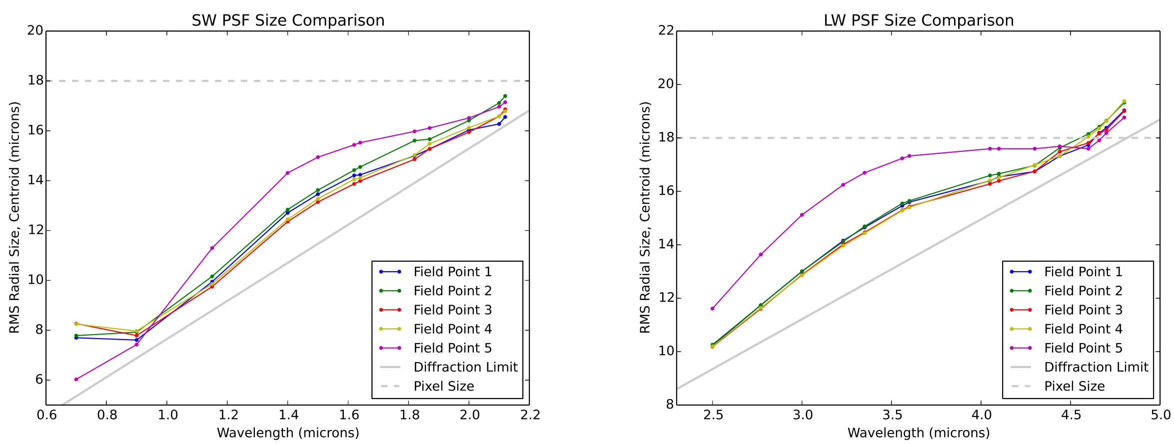

Figure 11: Plots of the PSF radial sizes as a function of wavelength for monochromatic sources at all five Zemax field points corresponding to the centers of the detectors.

6 Simulated Images

An example of a simulated NIRCam image is shown in Figure 12 using the following command:

```
./phosim examples/jwst/candels_phosim_bright.cat -c examples/jwst/noatmosphere -i nircam_lw
```

The catalog is the Hubble Space Telescope-based catalog with Sersic distributions for the galaxies. The commands turn off the atmosphere, but leaves all other physics on. No background was included in these images, although it is always possible to simulate background with the `quickbackground` CommandFile instead.

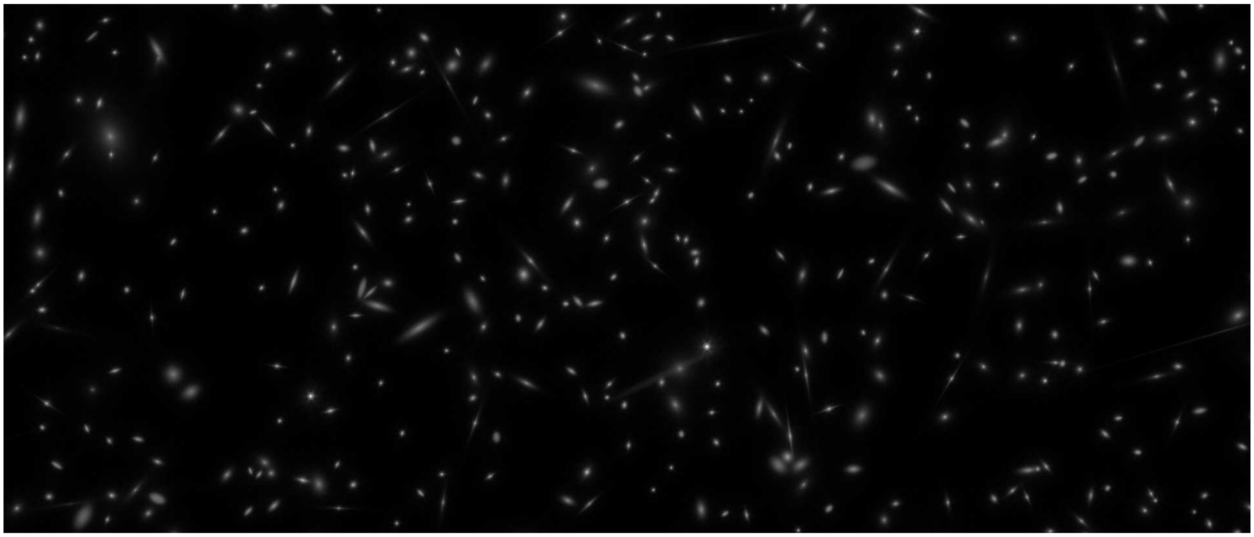

Figure 12: Close-up of a simulated LW NIRCam image.

7 Advantages of the PhoSim Approach

Other tools exist to model the behavior of NIRCam. The most useful are WebbPSF (Perren, 2012, 2014) and The Space Telescope Image Product Simulator (STIPS). WebbPSF takes pre-computed OPD files, and simulates the diffraction and detector resolution through the appropriate wavelength(s) for a selected filter. STIPS can then be used to generate a NIRCam image from a catalog of stars and galaxies. STIPS takes NIRCam PSFs generated from WebbPSF along with the JWST exposure time calculator, Pandeia, and outputs a simulated FITS image with some detector effects (STSci, 2017).

A user desiring to simulate an image in an end-to-end capacity would have to generate an OPD file with Zemax across the appropriate wavelengths with the desired defocus or use the limited pre-computed OPD library, use WebbPSF to obtain the PSF from the OPD with the appropriate filter, and use STIPS to simulate the entire desired catalog. Instead, PhoSim presents a comprehensive, physics-based package to do all of this with one command. PhoSim simlifies the process and likely produces more realistic images (e.g., full multi-wavelength dependence, field-dependent PSF, detector physics, future readout simulation). In addition, PhoSim's powerful physics CommandFile input presents the ability to analyze each component of the physics individually. For example, one could use PhoSim to investigate how large-angle scattering, dust contamination, cosmic rays, *etc.* effect a NIRCam image in great detail. Finally, PhoSim can easily be scaled to grid-computing. For these reasons, this work is expected to be of great interest to the JWST/NIRCam community both for planning observations and analysis of the optical system itself.

8 Future Work

Along with more widespread use of PhoSim for NIRCam purposes, a more comprehensive validation needs to be done. For examples, after OTIS and in-orbit testing, more work can be done to accurately calibrate this work with the real telescope. Future high-priority calibration efforts include the exact chip positions/defocus.

In general, PhoSim is capable of much more details than are described here. Some examples of further improvements and validation include:

- Realistic NIRCam readout simulation.
- Angle-dependent indices of refraction.
- Perturbation models.
- Modifications to cosmic ray physics for space.
- More detailed detector parameters (readout noise, well depth, *etc.*) for each module.
- Throughput curves on each individual optical component including angle dependence.
- Implementation of coronagraph masks and wedges.
- Wavefront sensor, spectroscopic (grism), and calibration source modes.
- More detailed PSF analysis and calibration of detector defocus and other parameters with OTIS and in-orbit testing.
- Astrometric and throughput validation.

9 Acknowledgements

Thanks to Eiichi Egami, Jarron Leisenring, and Marcia Rieke at the University of Arizona for their contributions and clarifications in support of this work. Many thanks to John R. Peterson at Purdue University for advising this project and creating PhoSim.

References

Burke, C. PhoSim Internal Document (PIN-23) (2017) <http://lsst.rcac.purdue.edu/doc/diffraction_doc_final.pdf>.

Chu, J. et al. *J Appl. Phys.* (1994)

Dornhaus, R.et al. *Springer* (1983)

Finkman, E., and Schacham, S. E. *J. Appl. Phys.* (1984)

Gardner, J. P. et al. *Space Sci. Rev.* (2006)

Garnett, J. D. et al. *Proc. SPIE* (2004)

Greene, T. *Proc. SPIE* (2010)

Hansen, G. L. et al. *J. Appl. Phys.* (1982)

Hougen, C. A. *J. Appl. Phys.* (1989)

Itsuno, A. M. *Dissertation* (2012)

Knight, S. J. et al. *Proc. SPIE* (2012)

Loose, M. *Proc. SPIE* (2007)

Lui, K. et al. *J. Appl. Phys.* (1994)

Peterson, J. R. et al. *Astrophys. J* (2015)

Perren, M. D. et al. *Proc. SPIE* (2012)

Perren, M. D. et al. *Proc. SPIE* (2014)

Radiant ZEMAX LLC “ZEMAX User’s Manual.” (2011)

Rieke, M. “NIRCam Sensitivity Calculations” *Techincal Report, NASA CSFC* (2013)

Rogalski, A. *Rep. Prog. Phys.* (2005)

Rosbeck, J. P. et al. *J. Appl. Phys.* (1982)

Sellmeier, W. *Ann. Phys. Chem.* (1871)

Space Telescope Science Institute *Website* (2017) <http://www.stsci.edu/jwst/instruments/nircam>.

Space Telescope Science Institute *Website* (2017) <http://www.stsci.edu/wfirst/software/STIPS>.

10 Appendix

Table 7: SW optics data [all units in mm unless otherwise noted].

name	type	R	outer radius	inner radius	κ	coating file	medium file
PM	mirror	15879.72199999988776	3302.6	705.0	-0.9966605	none	vacuum
SM	mirror	1778.912670000002707	369.0	0.0	-1.65981	none	vacuum
TM	mirror	3016.226999999546513	351.0	0.0	-0.6595364	none	vacuum
FSM	mirror	0.0	86.25	0.0	0.0	none	vacuum
POM	mirror	1554.999999999896665	63.15	0.0	0.0	none	vacuum
COM1	lens	1106.499999999999960	57.28391538309	0.0	0.0	none	vacuum
COM2	lens	0.0	57.25668763758	0.0	0.0	none	vacuum
FFF	mirror	475281.9971999999522	46.81130624037	0.0	0.0	none	vacuum
col11	lens	122.9010899999999949	43.5	0.0	0.0	none	`ZnSe_37K.txt`
col12	lens	136.6041800000000103	43.47145432290	0.0	0.0	none	vacuum
col21	lens	-184.2484099999999985	43.44337081677	0.0	0.0	none	`BaF2_37K.txt`
col22	lens	0.0	42.46851437788	0.0	0.0	none	vacuum
col31	lens	0.0	41.99857765475	0.0	0.0	none	`LiF2_37K.txt`
col32	lens	-1096.182019999999991	41.00225312677	0.0	0.0	none	vacuum
DBS	mirror	0.0	31.6578662976	0.0	0.0	none	vacuum
SWP1	lens	0.0	24.0	0.0	0.0	none	vacuum
SWP2	lens	0.0	21.0	0.0	0.0	none	vacuum
SWF1	filter	0.0	24.0	0.0	0.0	FILTER	`F_Silica.txt`
SWF2	filter	0.0	24.0	0.0	0.0	none	vacuum
SW11	lens	-64.891679999999996333	29.1	0.0	0.0	none	`LiF2_37K.txt`
SW12	lens	-92.927250000000000778	40.85	0.0	0.0	none	vacuum
SW21	lens	-309.96435000000002353	40.85	0.0	0.0	none	`BaF2_37K.txt`
SW22	lens	-81.079639999999997920	40.85	0.0	0.0	none	vacuum
SW31	lens	-68.879400000000001980	40.85	0.0	0.0	none	`ZnSe_37K.txt`
SW32	lens	-80.548100000000003283	40.85	0.0	4.236517e-3*	none	vacuum
SFF	mirror	0.0	42.76310350875	0.0	0.0	none	vacuum
SWFPM	mirror	0.0	65.31171316080	0.0	0.0	none	vacuum
SWFPA	det	0.0	55.72072050086	0.0	0.0	none	vacuum

*SW32 has higher order aspheric coefficients, $a_1 = 0.0, a_2 = -4.151469\text{e}{-12}, a_3 = 0.0, a_4 = -7.357185\text{e}{-16}$, $a_5 = 0.0, a_6 = 6.843002\text{e}{-19}, a_7 = 0.0, a_8 = -1.958396\text{e}{-22}$ [in m].

Table 8: LW optics data [all units in mm unless otherwise noted].

name	type	R	outer radius	inner radius	κ	coating file	medium file
PM	mirror	15879.72199999988776	3302.6	705.0	-0.9966605	none	vacuum
SM	mirror	1778.912670000002707	369.0	0.0	-1.65981	none	vacuum
TM	mirror	3016.226999999546513	351.0	0.0	-0.6595364	none	vacuum
FSM	mirror	0.0	86.25	0.0	0.0	none	vacuum
POM	mirror	1554.999999999896665	63.15	0.0	0.0	none	vacuum
FFF	mirror	475281.9971999999522	46.81130624213	0.0	0.0	none	vacuum
col11	mirror	0.0	86.25	0.0	0.0	none	vacuum
col12	lens	136.6041800000000103	43.35479374842	0.0	0.0	none	vacuum
col21	lens	-184.2484099999999985	43.3086027514	0.0	0.0	none	`BaF2_37K.txt`
col22	lens	0.0	42.3444940007	0.0	0.0	none	vacuum
col31	lens	0.0	41.89314247646	0.0	0.0	none	`LiF2_37K.txt`
col32	lens	-1096.182019999999991	40.88842822985	0.0	0.0	none	vacuum
DBS1	lens	0.0	31.79786904571	0.0	0.0	none	`Si_30K.txt`
DBS2	lens	0.0	32.15700401958	0.0	0.0	none	vacuum
LWP1	lens	0.0	17.97842394889	0.0	0.0	none	vacuum
LWP2	lens	0.0	17.49913283627	0.0	0.0	none	vacuum
LWF1	filter	0.0	17.83715226261	0.0	0.0	FILTER	`Si_30K.txt`
LWF2	filter	0.0	18.02019641833	0.0	0.0	none	vacuum
LW11	lens	42.274799999999999990	24.0	0.0	0.0	none	`LiF2_37K.txt`
LW12	lens	57.025900000000000023	23.24667628549	0.0	0.0	none	vacuum
LW21	lens	454.6290200000000561	24.65014075324	0.0	0.0	none	`BaF2_37K.txt`
LW22	lens	59.900590000000000634	26.06114241729	0.0	0.0	none	vacuum
LW31	lens	57.085599999999999757	25.85334537745	0.0	0.0	none	`ZnSe_37K.txt`
LW32	lens	66.393399999999999967	28.43158531549	0.0	-.017627939*	none	vacuum
LWFPM	mirror	0.0	37.3	0.0	0.0	none	vacuum
LWFPA	det	0.0	27.23884760803	0.0	0.0	none	vacuum

*LW32 has higher order aspheric coefficients, $a_1 = 0.0, a_2 = 1.004637\text{e}{-11}, a_3 = 0.0, a_4 = 3.813024\text{e}{-15}$, $a_5 = 0.0, a_6 = -1.425781\text{e}{-18}, a_7 = 0.0, a_8 = 6.494986\text{e}{-22}$ [in m].

Table 9: SW body commands.

name	type	value	surface link
SMyz	z	7169.041556	1
TMy	y	-0.186	2
TMz	z	-796.2719229	2
FSMy	y	-2.356548	3
FSMz	z	1047.8479	3
POMx	x	-54.763138	4
POMy	y	-306.8260525	4
POMz	z	-1889.00247	4
POMphi	ϕ	0.16477716547	4
POMtheta	θ	5.98158192792	4
COM1x	x	-60.44363216	5
COM1y	y	-278.5587445	5
COM1z	z	-1836.947849	5
COM1phi	ϕ	0.232653289929	5
COM1theta	θ	5.81099613362	5
COM2x	x	-60.60510071	6
COM2y	y	-277.7323020	6
COM2z	z	-1835.447814	6
COM2phi	ϕ	0.250289891876	6
COM2theta	θ	5.84387276753	6
FFFx	x	-112.4997852	7
FFFy	y	-68.06801796	7
FFFz	z	-1445.119442	7
FFFphi	ϕ	1.84950606131	7
FFFtheta	θ	6.21522201243	7
col11x	x	-112.4997609	8
col11y	y	-15.39201908	8
col11z	z	-1535.583489	8
col12x	x	-112.4997342	9
col12y	y	-8.951113961	9
col12z	z	-1546.644896	9
col21x	x	-112.49973	10
col21y	y	-7.944722537	10
col21z	z	-1548.373241	10
col22x	x	-112.4996935	11
col22y	y	0.861202427	11
col22z	z	-1563.49626	11
col31x	x	-112.4996852	12
col31y	y	2.873985276	12
col31z	z	-1566.95295	12
col32x	x	-112.499662	13
col32y	y	8.459457682	13
col32z	z	-1576.545264	13
colphi	ϕ	3.14158850968	8 9 10 11 12 13
coltheta	θ	5.75589249333	8 9 10 11 12 13
DBSx	x	-112.4993949	14
DBSy	y	72.91882842	14
DBSz	z	-1687.245759	14
DBSphi	ϕ	8.05395133621e-05	14
DBStheta	θ	6.19913753355	14
SWP1x	x	-112.5008108	15
SWP1y	y	140.8320901	15
SWP1z	z	-1605.857587	15
SWP2x	x	-112.5010553	16
SWP2y	y	144.0349029	16
SWP2z	z	-1602.018058	16
SWP2phi	ϕ	7.63488254694e-05	15 16
SWP2theta	θ	5.58795465925	15 16
SWF1x	x	-112.501716	17
SWF1y	y	152.6889032	17
SWF1z	z	-1591.643648	17
SWF2x	x	-112.1533363	18
SWF2y	y	155.8920048	18
SWF2z	z	-1587.820198	18
SWFphi	ϕ	6.17484792051	17 18
SWFtheta	θ	5.58294919421	17 18
SW11x	x	-112.3993282	19
SW11y	y	192.0069524	19
SW11z	z	-1544.533083	19
SW12x	x	-112.3997195	20
SW12y	y	197.1314529	20
SW12z	z	-1538.389835	20
SW21x	x	-112.4019717	21
SW21y	y	226.6306891	21
SW21z	z	-1503.02617	21
SW22x	x	-112.4029449	22
SW22y	y	239.3778843	22
SW22z	z	-1487.744841	22
SW31x	x	-112.4032403	23
SW31y	y	243.2460507	23
SW31z	z	-1483.107686	23
SW32x	x	-112.4038271	24
SW32y	y	250.9328016	24
SW32z	z	-1473.892814	24
SWphi	ϕ	7.63488254694e-05	19 20 21 22 23 24
SWtheta	θ	5.58795465925	19 20 21 22 23 24
SFFx	x	-112.4088339	25
SFFy	y	316.5102378	25
SFFz	z	-1395.278628	25
SFFphi	ϕ	7.79148113408e-05	25
SFFtheta	θ	6.06986291776	25
SWFPMx	x	-112.417206	26
SWFPMy	y	437.3926173	26
SWFPMz	z	-1834.473555	26
SWFPMphi	ϕ	1.83028704458	26
SWFPMtheta	θ	5.46249559392	26
SWFPAx	x	-237.3791782	27
SWFPAy	y	437.4607357	27
SWFPAz	z	-1834.434876	27
SWFPAphi	ϕ	1.53840832903	27
SWFPApsi	ψ	4.4739624637	27
SWFPAtheta	θ	4.710597624	27

Table 10: LW body commands.

name	type	value	surface link
SMz	z	7169.041556	1
TMy	y	-0.186	2
TMz	z	-796.2719229	2
FSMy	y	-2.356548000	3
FSMz	z	1047.847900	3
POMx	x	-54.76313800	4
POMy	y	-306.8260525	4
POMz	z	-1889.002471	4
POMphi	ϕ	0.16477716547	4
POMtheta	θ	5.98158192792	4
FFFx	x	-112.4997852	5
FFFy	y	-68.06801797	5
FFFz	z	-1445.119442	5
FFFphi	ϕ	1.84950606131	5
FFFtheta	θ	6.21522201243	5
col11x	x	-112.4997609	6
col11y	y	-15.39201909	6
col11z	z	-1535.583489	6
col12x	x	-112.4997342	7
col12y	y	-8.951113973	7
col12z	z	-1546.644896	7
col21x	x	-112.4997300	8
col21y	y	-7.944722549	8
col21z	z	-1548.373241	8
col22x	x	-112.4996935	9
col22y	y	.8612024152	9
col22z	z	-1563.496260	9
col31x	x	-112.4996852	10
col31y	y	2.873985264	10
col31z	z	-1566.952950	10
col32x	x	-112.4996620	11
col32y	y	8.459457670	11
col32z	z	-1576.545264	11
colphi	ϕ	3.14158850968	6 7 8 9 10 11
coltheta	θ	5.75589249333	6 7 8 9 10 11
DBS1x	x	-112.4993949	12
DBS1y	y	72.91882841	12
DBS1z	z	-1687.245759	12
DBS2x	x	-112.4992935	13
DBS2y	y	71.65959557	13
DBS2z	z	-1702.192810	13
DBSphi	ϕ	8.05395133621e-05	12 13
DBStheta	θ	6.19913753355	12 13
LWP1x	x	-112.4999297	14
LWP1y	y	123.7925201	14
LWP1z	z	-1787.555472	14
LWP2x	x	-112.4983746	15
LWP2y	y	126.3078625	15
LWP2z	z	-1791.876704	15
LWPphi	ϕ	3.14097440425	14 15
LWPtheta	θ	5.75603959334	14 15
LWF1x	x	-112.4941727	16
LWF1y	y	133.1043178	16
LWF1z	z	-1803.552674	16
LWF2x	x	-112.1439979	17
LWF2y	y	135.6225741	17
LWF2z	z	-1807.857992	17
LWFphi	ϕ	3.00342416494	16 17
LWFtheta	θ	5.74974659872	16 17
LW11x	x	-112.2190553	18
LW11y	y	157.1706992	18
LW11z	z	-1844.908291	18
LW12x	x	-112.2167226	19
LW12y	y	160.9437129	19
LW12z	z	-1851.390139	19
LW21x	x	-112.2149908	20
LW21y	y	163.7449286	20
LW21z	z	-1856.202488	20
LW22x	x	-112.2095012	21
LW22y	y	172.6240874	21
LW22z	z	-1871.456438	21
LW31x	x	-112.2082572	22
LW31y	y	174.6363614	22
LW31z	z	-1874.913424	22
LW32x	x	-112.2052091	23
LW32y	y	179.5664326	23
LW32z	z	-1883.383040	23
LW32phi	ϕ	3.14097440425	18 19 20 21 22 23
LW32theta	θ	5.75603959334	18 19 20 21 22 23
LWFPMx	x	-112.1332923	24
LWFPMy	y	295.8898027	24
LWFPMz	z	-2083.220768	24
LWFPMphi	ϕ	2.03660358779	24
LWFPMtheta	θ	5.36957399386	24
LWFPAx	x	-198.1410122	25
LWFPAy	y	295.9836497	25
LWFPAz	z	-2083.298528	25
LWFPAphi	ϕ	1.55435694024	25
LWFPApsi	ψ	4.2155523449	25
LWFPAtheta	θ	4.7151199699	25